Mechanistic origin of the enhanced strength and ductility in Mg-rare earth alloys

Henry Ovri[1*], Jürgen Markmann[1], Juri Barthel[2], Maximilian Kruth[2], Hajo Dieringa[3], Erica T. Lilleodden[4]

[1]Helmholtz Zentrum Hereon, Institute of Materials Mechanics, 21502 Geesthacht, Germany.
[2]Ernst Ruska-Centre (ER-C 2) Forschungszentrum Juelich GmbH, 52425 Juelich, Germany
[3]Helmholtz Zentrum Hereon, Institute of Material and Process Design, 21502 Geesthacht, Germany.
[4]Fraunhofer Institute for Microstructure of Materials and Systems, 06120 Halle, Germany

Abstract

Magnesium (Mg) alloys with low concentrations of rare earth additions are known to exhibit strengths and ductility that are significantly higher than those obtained in traditional Mg alloys. However, the mechanisms that underlie these improvements are still open to debate. We assessed these mechanism(s) by carrying out in-depth analysis of the deformation behaviour in single crystals of pure Mg and a homogenized Mg–0.75 at.% Gd alloy oriented for twinning, pyramidal- and basal-slip. We observed a fivefold increase in basal CRSS, an eightfold increase in twinning CRSS and a fourfold decrease of the pyramidal/basal CRSS (P/B) ratio due to Gd addition. We also observed that while twinning and pyramidal slip activities were similar in the two material systems, basal slip was radically different. Specifically, basal slip was planar in the alloy but wavy in pure Mg. Our work reveals that these observations are a consequence of Gd-rich short-range ordered (SRO) clusters in the alloy. We show that interactions between dislocations and the SRO clusters would lead to significant increases in strength and $\langle c + a \rangle$ slip activity, and consequently, ductility improvements in homogenized polycrystalline Mg-Gd alloys.

Keywords: Mg-Gd; Mg-RE; microcompression; planar slip; STEM; short range order; SAXS

1 Introduction

The utility of classical wrought Mg alloys, i.e. the AZ, ZK and AM series, in lightweight structural applications is limited by their comparatively poor room temperature ductility and low yield strength. The origin of the poor ductility has been partly traced to the strong plastic anisotropy of the hexagonal close packed (HCP) crystal structure of Mg [1]. Specifically, the low critical resolved shear stress (CRSS) of basal slip (~ 0.5 MPa) [2] together with the significantly high nonbasal/basal slip ratios (60–100) [3-5] in HCP Mg promotes strong basal texture and consequently low ductility in these alloy systems. Conversely, various empirical [6-8] and computational efforts [9-11] indicate that low/medium concentrations of rare earth (RE) solutes in Mg weakens the deleterious basal Mg texture, and significantly enhances room temperature ductility and strength.

Different mechanistic models have been proposed to explain the enhanced ductility in Mg-RE based alloys. For instance, Wu et al. [12], argue that low concentrations of REs lower the activation energy barrier for the cross slip of pyramidal II dislocations to pyramidal I planes (ΔG_{xs}), thereby circumventing the inimical pyramidal II-to-basal transition. The reduction of ΔG_{xs} is thus accompanied by increased $\langle c+a \rangle$ activity, which provides the much needed $\langle c \rangle$-axis deformation component that satisfies the von Mises criterion for homogeneous deformation in polycrystals, and consequently improved ductility [13]. However, experimental evidence provided later in this work does show remarkable similarity between $\langle c+a \rangle$ dislocations configurations in pure Mg and the Mg-RE alloy investigated herein; an indication that the lowering of the ΔG_{xs} does not underlie the increased $\langle c+a \rangle$ activity and correspondingly, the improved ductility associated with the Mg-RE based alloys. Other workers [14-16] suggest that the RE elements promote the reduction of the intrinsic stacking fault (ISF) energy, with the resulting stacking faults acting as heterogeneous nucleation sites for $\langle c+a \rangle$ dislocations. However, Ahmad et al. [17] argues that the stresses required for the nucleation and existence of the prior ISF are not easily met and therefore unlike to occur. Yet another group of authors [18-20] propose that the large difference in atomic radius between RE and Mg atoms causes a strong solute drag effect, i.e. dynamic strain aging (DSA), which promotes texture weakening and enhances ductility in Mg-RE based alloys. However, it is highly unlikely that the enhanced room temperature ductility in Mg-REs is associated with DSA because experimental evidence only supports the occurrence of DSA in these alloy systems at elevated temperatures [18-21].

The foregoing discussion indicates that the mechanistic origin of the enhanced ductility in these alloy systems is still been debated. Additionally, whereas the solute strengthening potential of rare earth additions in Mg is well-established [22-24], the underlying mechanism(s) that govern strengthening in these materials systems are also yet to be fully established. For example, Miura et al.[22], who performed experiments on single crystals of Mg-REs argue that the atomic size mismatch theory for solid solution strengthening cannot sufficiently explain the strength observed in the alloy. Other workers have also reached similar conclusions [10, 23]. Clearly, an understanding of these mechanisms is critical for the development of Mg alloys with improved ductility and strength.

We observe though that investigations aimed at unravelling the mechanisms underlying the enhanced ductility have mostly focussed on the role of the REs in solid solutions. Yet recent microstructural characterization with aberration-corrected high-angle annular dark-field scanning transmission electron microscopy (HAADF-STEM) and various modelling efforts do confirm the existence of a wide variety of short-range ordered solute clusters, GP zones and precipitates in several Mg-RE based alloys [25-29]. Whereas these solute clusters and GP zones have been largely shown to occur during

the early stages of artificial aging, a few workers have reported the existence of a family of short-range ordered solute clusters in homogenized Mg-Gd alloys [25, 30]. Short range ordering (SRO) refers to the preferential local segregation of elements to specific sites within a lattice and over spatial dimensions that are in the order of a few interatomic distances. SRO is known to cause significant strengthening in other metallic alloy systems because additional stress is required to destroy the order [31-35]. Accordingly, we expect that such solute clusters, if present, will have a strong influence on dislocation glide and/or twinning activities in Mg-Gd based alloys and by extension on their strength and ductility. It is therefore worthwhile to re-examine the influence of the REs with a view to determining whether such SRO clusters exist, establishing their structure and their effect on the mechanical response of these interesting alloy systems.

In order to contribute to the discourse, we employed a Small Angle X-ray Scattering (SAXS) device to probe the microstructure of a homogenized Mg–0.75 at.% Gd alloy for the presence of solute clusters or GP zones. X-ray diffraction based methods record scattered intensities at small scattering angles thus making it an ideal tool for the characterization of nanoscale structural and morphological information of the scatterers, more especially when the concentrations are low. Similar measurements were also done in a 99.85 at.% pure Mg sample. Further characterization of the solute clusters was achieved with atomic-resolution High-Angle Annular Dark-Field Scanning Transmission Electron Microscopy (HAADF-STEM). We then carried out in-depth characterization of the dislocation–obstacle behaviour in single crystals of both material systems oriented for twinning, basal-, and pyramidal-slip using a combination of microcompression testing and STEM measurements. Our observations provide new insights into the role of the REs in Mg alloy systems.

2 Experimental procedures

Both material systems, i.e. the 99.85 at.% pure Mg and the as-cast Mg–0.75 at.% Gd alloy, were heat treated at 450°C for 24 hours to promote homogenization and grain growth. The average grain size after the heat treatment was ~1 mm; this provided sufficient area for the subsequent fabrication of micropillars for microcompression testing.

X-ray measurements of the homogenized samples were carried out in a Xenocs Xeuss 3.0 (SAXS) laboratory beamline. The samples were ground down to ~ 600 µm thickness in order to facilitate x-ray measurements in transmission. A microfocus tube with a molybdenum anode operating at 50 kV and 1.0 mA served as x-ray source. The spot size on the sample was adjusted to 900 µm x 900 µm. The wavelength of 0.711 Å in combination with a sample thickness of 600 µm and a material consisting mainly of Mg results in a transmission between 65 and 70%. The SAXS device was equipped with a

DECTRIS PILATUS3 R 300K 2D x-ray detector with an increased efficiency for Mo x-ray radiation of ca. 70%. The chosen sample to detector distance was 200 mm and the total image size was 1341x1210 pixels of 172 μm in size each assembled from 12 detector images at different lateral positions in order to cover the total size and eliminate the dead areas of the detector. The samples were mounted in a standard SAXS sample holder fixed with scotch tape. The SAXS signal of the scotch tape was measured separately with the same parameters and subtracted from the measured patterns.

The high resolution HAADF-STEM measurements were done on a lamella excised from the alloy with a Ga^+ focused ion beam and were performed in a Thermofischer-FEI Spectra 300 electron microscope, operated at 200 kV accelerating voltage. A scanning electron probe of 0.1 nA current and 27.5 mrad semi-convergence angle was focused to full-width-at-half-maximum (FWHM) of about 0.7 at the surface of the cross-section sample using spherical aberration correction. STEM images were recorded from less than 100 nm thin cross-section samples with an annular dark-field (ADF) detector collecting electrons scattered into the angular range between 63 mrad to 200 mrad.

The samples used for the microcompression tests were prepared using standard metallography procedures. Afterwards, grains with index planes close to (0001), $(10\bar{1}2)$, and $(10\bar{1}0)$ planes, were identified in each of the material systems with electron backscatter diffraction (EBSD) method. These orientations were carefully chosen to ensure that $\langle c+a \rangle$ slip, $\langle a \rangle$ basal slip and tensile twinning, respectively, primarily accommodated deformation. The angle, Φ, between the plane normal to these orientations and the *c*-axis, the corresponding Schmid factors, SF, and the expected slip/twin systems in these orientations are given in Table 1**Error! Reference source not found.**.

Table 1: Planes and Schmid factors (SF) of the tested orientations

Mg-Gd		**Pure Mg**		**Expected slip /Twin**
Φ (deg)	**SF**	**Φ (deg)**	**SF**	
8	0.49	3	0.48	Pyramidal II
52	0.45	54	0.45	Basal
90	0.49	88	0.49	Tensile twin

Annular micropillars with a mid-plane diameter of ~ 15μm were then fabricated in the selected orientations with a focused (Ga+) ion beam (FIB) operating in an FEI Nova 200 dualbeam FIB/SEM microscope. The large pillar sizes were chosen to minimize size effects, i.e. the smaller is stronger phenomenon, that is known to occur in many material systems, including Mg [4], during

microcompression studies of single crystals. All the micropillars had aspect ratios (height to mid-plane diameter) between 2:1 and 3:1 to prevent buckling. The microcompression tests, at least three for each orientation, were conducted at room temperature in displacement-controlled mode using a Hysitron TI 980 Nanoindenter. All the microcompression tests were run to maximum strains between 7- 9% using a nominally constant strain rate of $5x10^{-5}$ s^{-1}. An engineering stress–strain analysis of the load (P)–displacement (h) measurements is applied herein, using the initial height and mid-diameter of the micropillars. Incipient plasticity is unfortunately a common feature in microcompression because of small misalignments between the micropillar surfaces and the flat punch indenter. This impedes the use of the conventional 0.2% strain offset criterion for the estimation of the yield strength. In view of this, we have adopted the approach for the estimation of yield strength from microcompression data prescribed by Kupka et. al [36]. Following their work, we define the yield strength as the stress at which the slope of the loading curve becomes less than 25% of the maximum loading stiffness $(\Delta P/\Delta h)$. The maximum loading stiffness corresponds with the point of full contact between pillar and punch.

Post mortem cross-sections used in the TEM examination were excised from the mid-section of the deformed pillars in both pure Mg and Mg-Gd with the FIB. Moreover, we excised cross sections from two orthogonal directions in the micropillars oriented for basal slip to facilitate a fuller virtualization of the dislocation structures. All the micrographs were taken in a Thermofisher-FEI Talos F200i microscope under various two-beam conditions in STEM mode. Besides, electron backscatter diffraction (EBSD) measurements were performed on the cross sections extracted from the micropillars oriented for twinning prior to final thinning for TEM measurement to establish the presence or absence of tensile twins.

3 Results and analysis

3.1 X-ray diffraction and HR-HAADF STEM measurements

2D x-ray intensity maps of the homogenized pure Mg and Mg-Gd samples are presented in Figure 1(a) and (b), respectively. The lateral positions on the detector are already transformed into corresponding components of the scattering vector, *Q*, since the sample to detector distance and wavelength are known. In case of such low detector distances, the approximation of the scattering vector lying in the detector plane becomes violated. The correction causes the distortions observed in the edges of these intensity maps. The reduced 1D spectrum of the homogenized Mg-Gd sample, together with the reference peak positions of pure Mg, is shown in Figure 1(c). Close examination of the homogenized Mg-Gd alloy 2D map reveals the existence of diffuse intensity maxima that are characteristic of superlattice reflections that arise from ordered phases [37]. The symmetry of this pattern (which

extends even to higher orders) obviously originates from the crystal lattice of one dominant grain in the illuminated volume. The position of the maxima are highlighted in the map with red open circles for easy visualization. The absence of these local maxima in the intensity map of the pure Mg sample is a strong indication that they are produced by structures other than the Mg matrix. We note that the distribution of the maxima in the Mg-Gd sample closely match the Ni_3Sn type superlattice reflections in the electron diffraction pattern arising from solute clusters in a Mg–5 at.% Gd alloy [38]. Furthermore, the approximate difference between the central spot and the scattered intensity maxima corresponds to orderings with periodicities of $2\pi/Q \approx 0.364\ nm$, while the width of the intensity maxima corresponds to a domain size of ~1.6 nm, as determined by a rough application of the Scherrer equation on the reduced data of two opposing 30° sectors of the 2D picture. These values are in excellent agreement with those obtained for the ordered clusters observed in the Mg-5 at.% Gd [38], and in Mg-Nd and Mg-Y alloys [25, 26] with a the aid of aberration-corrected HAADF-STEM. Further analysis of the actual SAXS regime close to the primary beam did not yield any findings. Increasing the sample to detector distance and even changing the wavelength by using a Cu x-ray source in order to increase the resolution of the device did not reveal any significant signal in the small-angle regime. Obviously, the average electron density of the observed ordered domains despite their different composition does not provide sufficient contrast to the electron density of the Mg matrix. Nevertheless, the measurements clearly points to the existence of a SRO phase in the homogenized Mg-Gd alloy.

Additional evidence for the existence of SRO clusters can be seen in the atomic resolution HAADF-STEM micrograph presented in Figure 1(d). The image was taken with the electron beam parallel to $[0001]_{\mathrm{Mg}}$ direction. The region within the blue box in the HR-HAADF-STEM image was further processed with the denoising/background-removal/super-resolution algorithm in the AtomSegNet App for atomic-resolution images developed by Lin et. al. [39] and is presented in Figure 1(e). Bright spots corresponding to Gd-rich atom columns parallel to the $[0001]_{Mg}$ direction can be clearly seen in the micrographs. Additionally, isolated SRO clusters comprising of a series of Gd-rich atom columns arranged in zigzag patterns and others consisting of two Gd rich atom columns situated at the opposite corners of a hexagon are easily identifiable in the micrographs. Examples of these isolated SRO clusters are highlighted with solid red and dashed red spheres, respectively, in the micrographs. The configuration of these SRO clusters exactly match those observed in other Mg-RE alloy [25, 26, 38]. Moreover, the column separation distance between the oppositely situated Gd-rich atom columns is $0.37\ nm$, which is in excellent agreement with the periodicity of the order determined by the x-ray measurement above. This gives further credence to the main finding made by the x-ray measurements, namely, that SRO phases exist in homogenized Mg-Gd alloy.

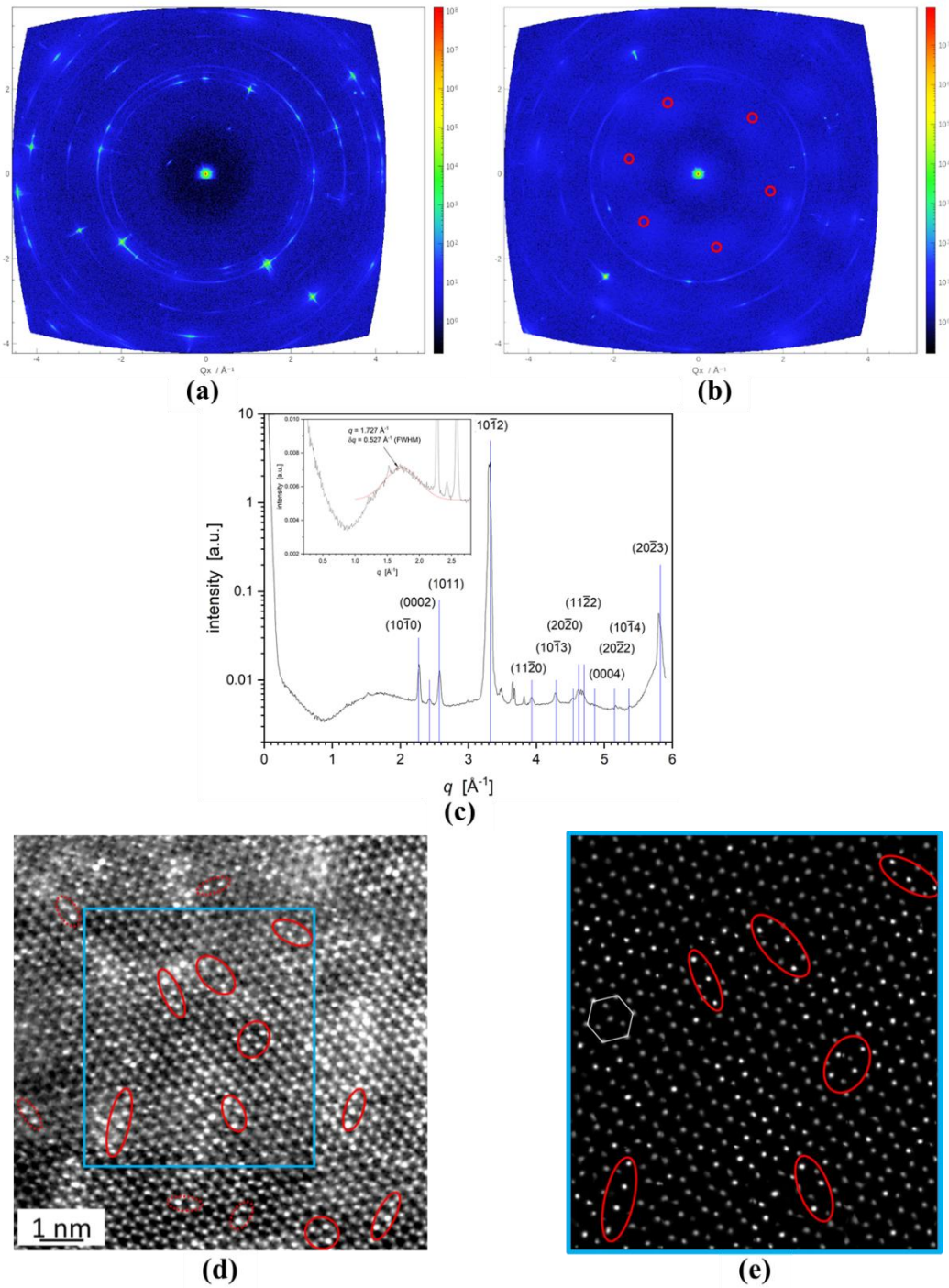

Figure 1: 2D intensity maps of (a) pure Mg and (b) homogenized Mg-Gd. The positions of the maxima are highlighted with red circles. (c) Reduced x-ray data of two opposing 30° sectors for the alloy together with Mg reference positions [40] and an inset showing the analysis of the diffuse peak of the ordered domain.(d) HR HAADF-STEM image showing a range of isolated solute clusters (highlighted with red spheres) in the Mg-Gd alloy. The image was taken with the electron beam parallel to $[0001]_{Mg}$ *direction. (e) is region within the blue box in (d) after post processing. A hexagonal ring that corresponds to the HCP unit cell is highlighted in the image.*

3.2 Deformation behaviour in micropillars oriented for basal slip

Representative engineering stress vs strain curves obtained from the basal slip favourable orientations are shown in Figure 2. Two curves are presented for each metal system. Both pure Mg and Mg-Gd alloy show a distinct increase in stress until yield followed by a slight strain hardening. A few stochastic stress drops can also be seen in the post-yield curves. These are likely associated with the activation and release of slip bands during deformation. The pure Mg pillars yielded at a CRSS of 3.6 MPa, which is about seven times the expected CRSS for basal slip in Mg [41]. The high CRSS is most likely a combination of size effect, which is consistently observed in microcompression experiments, and solute strengthening from impurity atoms in the pure Mg samples. Regardless, we note that the CRSS value reported here is comparatively lower than values reported by other researchers [8, 42] for basal slip in pure Mg and consequently closer to the bulk single crystal CRSS value. Apparently, the ominous size effect is significantly minimized by the use of micropillars with diameter of ~15µm. Moreover, the CRSS for the alloy is 16.1±2 MPa. In comparison to the CRSS for basal slip in the pure Mg samples, this represents about fivefold strengthening of the basal plane by the Gd atoms. Conversely, Wang et al [43], reports basal strengthening of less than twofold for 7µm diameter micropillars in the Mg–9 at.% Al and Mg–2 at.% Zn alloys they tested. The basal strengthening observed herein for the dilute Mg–Gd is thus consistent with other reports that show that rare earth elements additions do significantly increase the CRSS for basal slip [10, 22, 23].

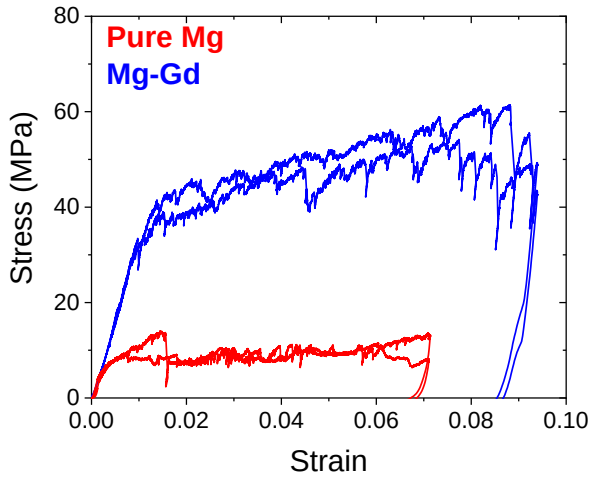

Figure 2: Representative engineering stress vs strain response of micropillars oriented for basal slip in pure Mg (in red) and the Mg-Gd alloy (in blue). Plots of two different tests are shown for each material.

A representative micropillar deformed in this orientation is shown in Figure 3 (a). A schematic that shows the orientations of examined lamellae slices is superimposed on the figure. We note that each lamellae slice, labelled S1 and S2, were excised from different micropillars even though their orientation is shown in the same figure. Characteristic slip steps that are well aligned with the basal

plane are visible in the figure; these were also observed in all the deformed pillars in this orientation. A micrograph showing the pre-deformation dislocation structure in the Mg-Gd alloy is shown in Figure 3 (b). The micrograph, which was taken under same two-beam conditions as the deformed micropillars, reveals that the alloy is largely dislocation free but contains a few precipitates that were most likely undissolved during the homogenization heat treatment. We opine that these will not alter the mechanical behaviour of the alloy since they are fairly large and sparsely dispersed.

Two-beam bright (BF) and dark (DF) field STEM micrographs showing the dislocation configuration in the orthogonal sectioned lamellae in the alloy are presented in Figure 3 (c-f), while those of pure Mg are shown in Figure 3 (g-i). The micrographs reveal significant differences between the dislocation configuration in the alloy and the pure Mg sample. Specifically, slip in the alloy is almost entirely planar and it is characterized by localized bands of straight dislocations that lie on the basal planes when viewed from the S1 slice with the $\{0\bar{1}11\}$ and $\{10\bar{1}0\}$ reflections near a $\langle 1\bar{2}1\bar{3}\rangle$ zone axis – see Figure 3 (c) and (d), respectively). The fact that the dislocations lie on the basal plane was also established by viewing the S2 lamella, i.e. Figure 3 (e&f). The basal planes, see dashed line in Figure 3 (f), lie at an angle to the plane of the paper in this slice. These micrographs, i.e. Figure 3 (e) and the magnified image in Figure 3 (f), clearly show that the dislocations bands lie mostly on the basal planes and are separated by dislocation-free islands. These micrographs were taken with the $\{0\bar{1}11\}$ reflection in a $\langle 2\bar{1}\bar{1}0\rangle$ zone axis. A schematic showing the arrangement of the dislocations within a band is also included in Figure 3 (f) for the purpose of clarity. Moreover, these dislocations have a purely basal $\langle a\rangle$ character since they were invisible with the (0002) reflection. According to the g.b invisibility criterion, dislocations with a $\langle 11\bar{2}0\rangle$ burgers vector, i.e $\langle a\rangle$ dislocations, are extinguished with a (0002) reflection.

Conversely, the dislocation configuration in the pure Mg samples consists of a high density of heavily curved (wavy) dislocations in the micropillars, see Figure 3 (g-i). Note that these micrographs were taken within same zone axes and under the same two-beam conditions described above for the alloy. In addition, dislocation loops and pairs of dislocations lobes, characteristic of end-on screw dislocations [44], abound in this orientation of the Mg sample. Examples of these are highlighted with a circle and arrows, respectively, in the high magnification two-beam DF insert in Figure 3 (g). These types of dislocation configurations were not observed in the alloy.

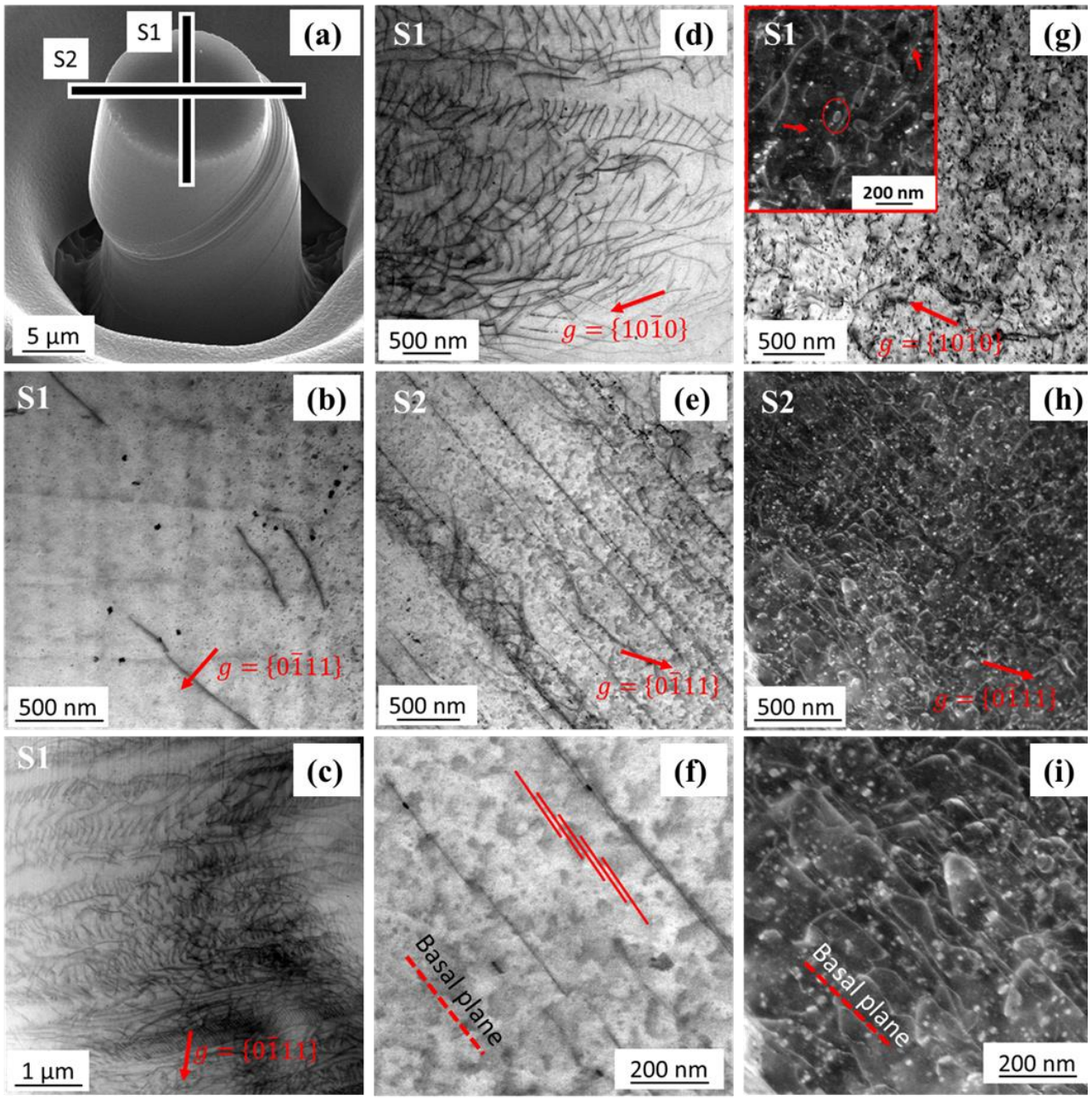

Figure 3: (a) SEM micrograph of a micropillar deformed in the basal orientation. TEM lamellae were excised from two orthogonal directions, S1 & S2, as shown schematically in the micrograph. Two-beam bright-field STEM images of the dislocation configuration in (b) undeformed MgGd; (c) – (f) deformed Mg-Gd alloy; (g) – (i) deformed pure Mg. Note that (f) & (i) are magnified images of (e) & (h), respectively. Moreover, (b),(c) and (d),(g) were taken near a $\langle 1\bar{2}1\bar{3} \rangle$ *zone axis with* $\{0\bar{1}11\}$ *and* $\{10\bar{1}0\}$ *reflections, respectively, while (e),(h) were taken near a* $\langle 2\bar{1}\bar{1}0 \rangle$ *zone axis with* $\{0\bar{1}11\}$ *reflections.*

We also note that there are no dislocation-free islands in the S2 slice of the pure Mg sample as was the case for the alloy; rather the dislocations are homogeneously distributed throughout the micropillar as

shown in Figure 3 (h). This stark difference is more easily recognizable upon comparing Figure 3 (f) and (i). Both images were taken with the $\{0\bar{1}11\}$ reflection and are higher magnification images of the micrographs shown in Figure 3 (e) and Figure 3(h), for the alloy and pure Mg, respectively.

3.3 Deformation behaviour in micropillars oriented for pyramidal slip

Figure 4(a) shows representative engineering stress-strain responses for micropillars oriented for pyramidal slip in the pure Mg and Mg-Gd samples. Both systems show very reproducible and similar stress-strain response, namely, a strong strain hardening after yielding until about 5% strain. Such high strain hardening has been reported for micropillars oriented for pyramidal slip in pure Mg [4]. We note however that the strain hardening in the alloy is higher than that of pure Mg. Moreover, the CRSS for pyramidal slip in the alloy (95±6 MPa) is only about 12% higher than that of pure Mg (85±2 MPa). The latter is consistent with CRSS values reported by other workers for pyramidal slip in pure Mg [4, 45, 46]. It is remarkable that the strengthening due to Gd in this orientation (1.1-fold) is significantly less than the approximately fivefold increase obtained in the basal orientation. Furthermore, a somewhat steep drop in stress was observed in all the curves after about 5-6% strain. Such a drop in stress is most likely associated with the deformation-mediated reorientation of the micropillars from the ab-initio pyramidal planes into orientations that are favourable for the activation of basal $\langle a \rangle$ slip. A stress drop would accompany such a reorientation since dislocation glide on the basal planes requires significantly less stress. The presence of slip traces that align with the basal slip direction in the deformed pillar, see Figure 4(b), support this thesis. Other workers [4, 8] have reported similar observations.

The dislocation configuration in the Mg-Gd and pure Mg samples are presented in Figure 4(c) and (d), respectively. Both micrographs were taken under two beam bright field conditions with a (0002) reflection near a $\langle 2\bar{1}\bar{1}0 \rangle$ zone axis. Figure 4(e) also shows the dislocation configuration of the alloy under a $\{0\bar{1}10\}$ reflection. We note, based on g.b invisibility criterion, that these dislocations are $\langle c + a \rangle$ type since they are visible under both reflections. Interestingly, the dislocation structures in both samples are strikingly similar unlike previously reported [12]. They both consist of short dislocation segments that appear to lie on the basal plane as shown by the basal plane trace, and large amounts of stepwise shaped dislocations that have been previously reported to be indicative of the double cross slip of dislocations between pyramidal II and pyramidal I planes [8, 47]. We were unable to unambiguously distinguish between pyramidal I and II slip in this work partly because the pyramidal-basal angles, i.e. the angles between the inclined dislocations and the basal plane trace, are not equal to the expected angles for pure screw dislocations in this orientation. This is an indication that the inclined dislocation segments are of mixed type. Nevertheless, it is apparent that the long

dislocation (inclined) segments in both samples lie predominantly on the pyramidal planes, suggesting that the same dislocation glide activities are operational in both material systems. Moreover, the pyramidal-basal angles in each of the samples are quite varied. This suggests that multiple pyramidal slip systems were activated during deformation and is consistent with Schmid factor analysis, which shows that at least four pyramidal II slip systems were activated in both samples. We also observed that there are a few precipitates with coffee-bean contrast in the deformed Mg-Gd sample. We posit that these precipitates are a result of strain-induced precipitation that apparently occurred after the microcompression experiments since they are not present in the undeformed microstructure taken with the same imaging conditions (Figure 4f). Our results and analysis hereafter are therefore unaffected by their presence. In the future, it would be worthwhile to investigate the influence of these strain-induced precipitates on the plasticity of the alloy.

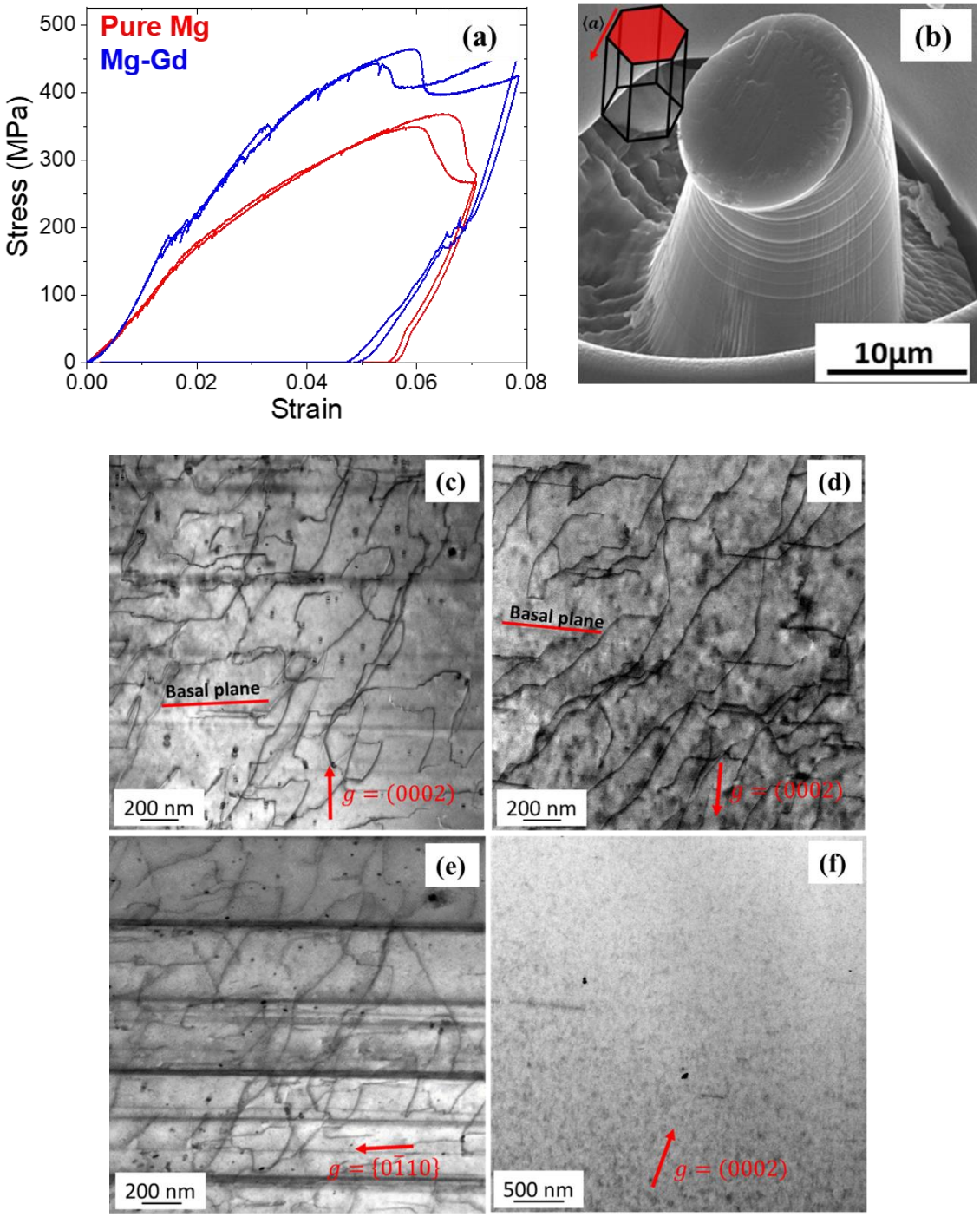

Figure 4: (a) Representative engineering stress vs. strain plot of micropillars set-up for pyramidal slip in pure Mg and Mg-Gd alloy. Plots of two different tests are shown for each material. (b) An SEM micrograph of a deformed micropillar in this orientation. Slip line traces that align with the basal plane are apparent. A schematic of the HCP unit cell showing the basal plane and slip direction is shown in the inserted in (b). Two beam bright field STEM images of Mg-Gd alloy (c) & (e) and pure Mg (d) after deformation. The microstructure of the undeformed Mg-Gd alloy is shown in (f). The micrographs in (c), (d) and (f) were taken near a $\langle 2\bar{1}\bar{1}0\rangle$ *zone axis with* (0002)*reflections, while (e) was taken with a* $\{0\bar{1}10\}$ *reflection.*

3.4 Deformation behaviour in micropillars oriented for twinning

The engineering stress-strain response obtained in the orientation where twinning preferentially occurred is shown in Figure 5(a). We see that the curves are also reproducible and that the trend between pure Mg and the alloy is similar. Both materials show a steady increase in stress until a CRSS of 63±4 MPa and 8±2 MPa, for Mg-Gd and pure Mg, respectively, is reached. This represents an eightfold increase of the CRSS for twinning that can be attributed to the Gd atoms. Apparently, strengthening associated with Gd atoms in this orientation is significantly higher than was observed in the basal and pyramidal orientations. These results are also consistent with observations made in Mg–Y alloys, where the twinning CRSS increased sharply from 45 MPa for 0.11 at.% Y addition to 113 MPa for Mg-1.13 at.% Y [8]. Comparatively, the CRSS for twinning in Mg-4 at.% Al and Mg-9 at% alloys showed increase of less than twofold [45]. These results thus strongly suggest that twinning is significantly delayed by RE additions.

An initial sharp drop in stress and thereafter, a strain hardening response that can be divided into two regimes that are marked by, weak and strong strain hardening, respectively, followed yielding in both material systems. A sharp drop in stress (or a strain burst in load controlled tests) in Mg pillars compressed along/near the $\{10\bar{1}0\}$ direction is commonly associated with the nucleation of $\{10\bar{1}2\}$ extension twins, while the weak strain hardening regime (or stress plateau in some cases) is associated with twin propagation across the deformed pillar. The transition from weak to strong strain hardening, which typically occurs at strains ranging from 5-6%, has been associated with twin saturation, i.e. the complete consumption of the deformed pillar with the twin, while the subsequent strain hardening likely arises from dislocation interactions within the reoriented pillar [42, 45].

Post mortem EBSD maps of cross sections excised from the Mg-Gd micropillars deformed to 3%, i.e. shortly after the initial stress drop, Figure 6(a), and ~8% strain, Figure 6(b), corroborate these explanations. The inverse pole figure (IPF) maps clearly show that the deformed area is almost completely consumed by $\{10\bar{1}2\}$ tensile twin after about 8% strain whereas only a small volume of the pillar twinned after about 3% strain. EBSD Orientation image (OIM) analysis of the measurements also confirm that the twinned regions are reoriented into a crystal orientation that is ~11° from the [0001] direction. Moreover, Schmid factor analysis indicates that further deformation within the fully twinned pillar will be predominantly accommodated by pyramidal slip. This analysis is supported by the STEM micrographs in Figure 7(a)-(c), which unambiguously show the presence of abundant $\langle c + a \rangle$ type dislocations.

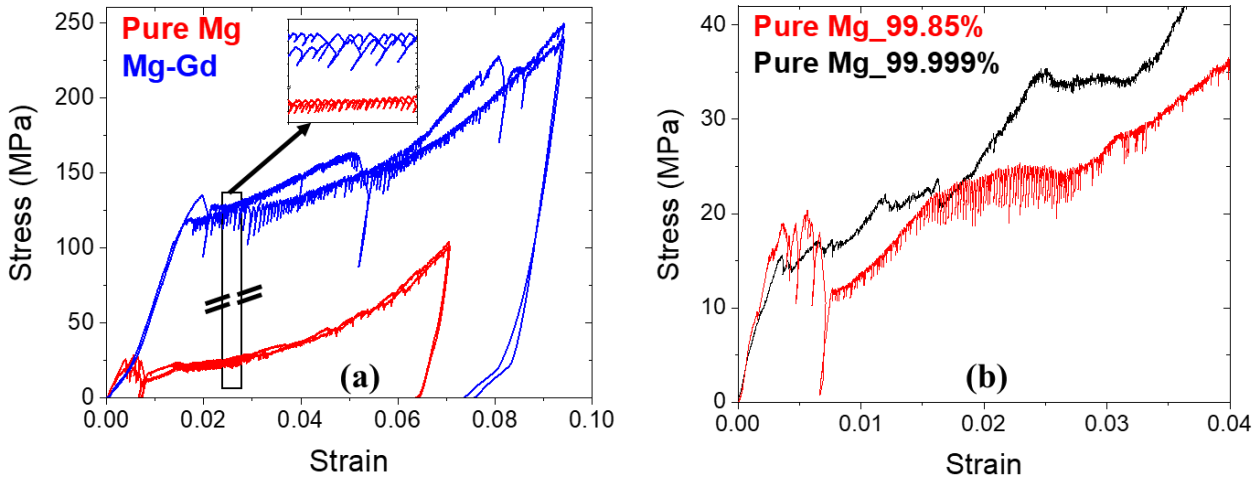

Figure 5: Stress vs strain response of micropillars preferentially oriented for twinning in (a) the pure Mg (in red) and Mg-Gd (in blue) sample. Plots of two different tests are shown for each material. The insert shows enlarged sections of the curves. (b) The pure Mg sample in (a) and an extremely pure Mg sample (in black).

We opine therefore that the stronger strain hardening observed in the second regime mentioned above is likely due to the dislocation interactions between cross-slipping pyramidal planes, and/or the dislocation debris left in the wake of the twins [4, 48]. We imagine that same mechanisms will be in operation in the pure Mg sample since the trend of the stress-strain response is similar for both material systems.

We also observed discrete post-yield stress drops, concomitant with the strain hardening. Interestingly, although the post-yield stress drops were observed in both Mg-Gd and pure Mg, the magnitude of the drops were significantly higher in the alloy. Similar observations has been reported in a Mg–9 wt.% Al alloy [45]. Whereas the origin of these stress drops is unclear, we can imagine that they are most likely associated with atom-scale interactions between diffusing solute atoms and the migrating twin boundary.

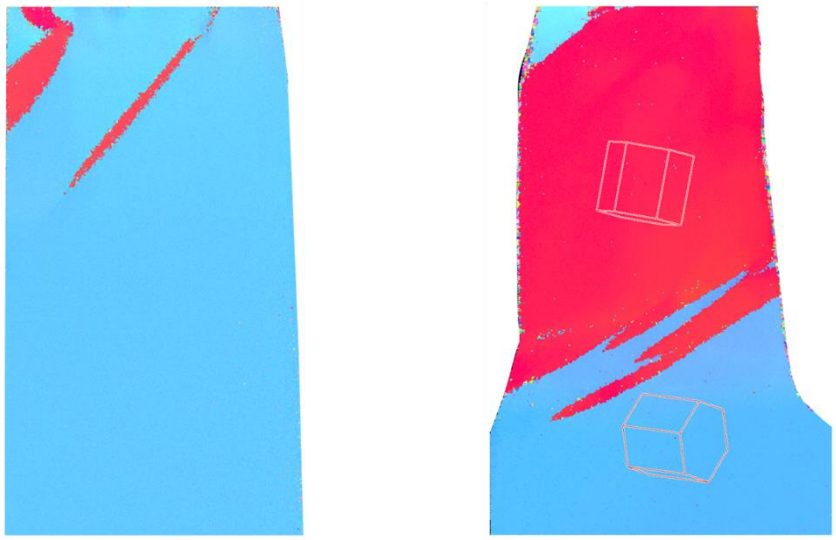

Figure 6: Superimposed EBSD inverse pole figure and image quality maps of cross sections excised from Mg-Gd micropillars deformed to (a) ~ 3% strain (b) ~ 8% strain.

This thesis is further supported by complimentary microcompression tests performed on a 99.999 at.% pure Mg– $[10\bar{1}0]$ oriented single crystal, compressed under the same conditions described earlier in section 2. As seen in Figure 5(b), there are hardly any stress drops in the higher purity pure Mg sample. This observation, in addition to the absence of such deterministic stress drops in the other orientation (compare Figure 2 and Figure 3a) strengthens the proposition that the stress drops are associated with interactions between solute/impurity atoms and twin boundaries. We will address the origin of such interactions in another publication.

We gained further insight into the deformation in this orientation by examining the 2B-BF STEM images obtained from the twinned regions in the Mg-Gd alloy (Figure 7 (a-c)) and the high purity pure Mg sample (Figure 7 (d-e)). The micrographs in Figure 7 (a, b, d & e) were taken with (0002) reflections, while Figure 7 (c & f) shows micrographs taken with $\{01\bar{1}1\}$ reflections. All these measurements were done near the $[2\bar{1}\bar{1}0]$ zone axes. The dislocation structure under the (0002) reflection in both material systems is mostly characterized by long rectilinear dislocations that span several hundred nanometres. These dislocations clearly lie on the basal planes but intermittently contain jogs. Since these dislocations are visible with a (0002) reflection, we can conclude, based on g.b criterion, that they are $\langle c \rangle$ containing dislocations. Additionally, the dislocations that lie along the basal plane in the pure Mg sample appear to contain loops that can be more clearly seen in the magnified image in Figure 7(d). These loops were only visible with the (0002) reflection and are also considered a signature of pyramidal glide [49]. A low angle grain boundary (LAGB) can also be seen

within the twin in the alloy. The dislocation structure within the LAGB is clearly revealed in the Figure 7(c). This micrograph indicates that the LAGB is effective in blocking dislocation glide and interrupting the stacking faults within the twin (see Figure 7(e)). Similar observations have been reported for other Mg alloys [8, 50, 51] but the origin and influence of such LAGB on plasticity is still open to debate and beyond the scope of this work.

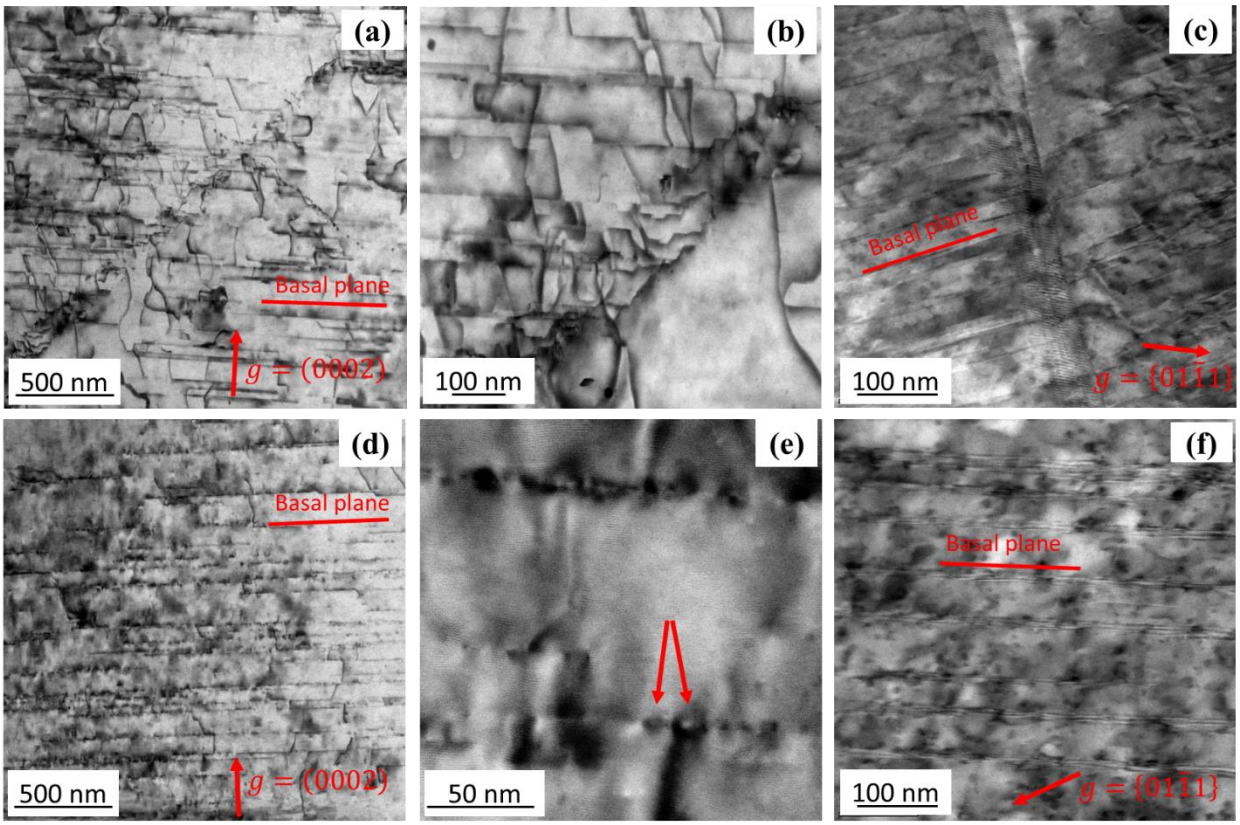

Figure 7: Two beam bright-field STEM images showing dislocation structures inside the twinned area in Mg-Gd (a-c) and in the 99.999% pure Mg sample (d-f). (b) & (e) are magnified sections of (a) & (d) respectively. Moreover, a, b, d, & e were taken with (0002) reflections while (c) & (f) where imaged with $\{01\bar{1}1\}$. *The basal plane trace in each reflection is highlighted in the micrographs. The two arrows in (e) highlight dislocation loops in the pure Mg sample.*

The dislocation structure under $\{01\bar{1}1\}$ reflections is shown in Figure 7 (e & f) for the alloy and pure Mg sample respectively. The microstructure under this reflection in both systems primarily consist of stacking faults (SF) that lie along the basal plane trace. These results are consistent with observations made by other workers [8, 48]. We note that the defect structures observed in both alloy and pure Mg in the twinning orientation are qualitatively similar except for the presence of the LAGB in the former.

4 Discussion

4.1 Underlying micromechanisms and their influence on the CRSS

As previously highlighted in section 3.2, dislocation glide in the alloy is apparently planar in the basal orientation, i.e., characterized by groups of long delineated dislocations that lie primarily on the basal plane, whereas it is wavy in pure Mg. The stark differences between the dislocation configuration in the basal orientation of the Mg-Gd and pure Mg sample strongly indicate that the underlying deformation mechanisms are not the same.

Planar slip is usually associated with the presence of atom-scale solute ordering (SRO) within solid solutions. Typically, dislocations in alloy systems with SRO domains tend to move in pairs within the active slip plane because the destruction of the atomic order, and consequently, the creation of an antiphase boundary (APB) in the glide plane by the leading dislocation in a pair, causes a lowering of the energy barrier. This makes it easier for successive dislocations to glide on same plane [32, 52]. A schematic of the atomic arrangement within a typical SRO cluster in Mg-RE alloys is shown in Figure 8(a). The existence of SRO clusters comprising of Gd-rich atom columns arranged in zigzag patterns as shown in the schematic has been clearly demonstrated by the x-ray diffraction and HR-HAADF-STEM measurements done in this work and presented in Figure 1. Figure 8(b) shows a schematic of the APB formed after one dislocation glides through such a cluster. Apparently, a second dislocation needs to glide through the plane to ensure a net zero change in order. The dislocation configuration in such systems is thus made up of dislocation pairs that are caused by the disruption and recreation of order, along with dislocation bands that are formed after the SRO domain is completely destroyed. Stoloff and Davies [52] argues further that the spacing within dislocations in a group are not the same and that neighbouring groups often have different signs. The dislocation configuration in the basal orientation of the alloy is extensively consistent with the preceding literature description of planar slip. For example, three dislocation pairs and a band with eleven dislocations are highlighted with blue arrows and a brace, respectively, in Figure 3(d). It is also apparent from Figure 3(c) and (d) that the dislocation spacing vary across the groups. Clear evidence that neighbour groups mostly have burgers vectors with different signs can also be seen in these micrographs. Note that other types of SRO configurations in these alloy systems would produce same effect.

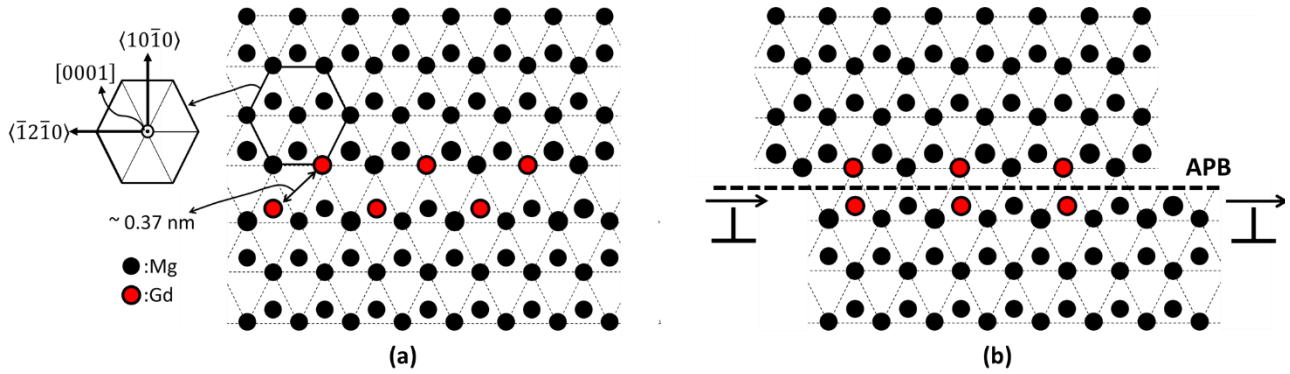

Figure 8: A schematic of (a) typical solute cluster in Mg-RE. (b) antiphase boundary (APB) formed after the glide of a single dislocation

Moreover, various workers [10, 23, 53] have shown that classical solid solution models cannot explain the high yield strength experimentally observed in the Mg-REs. It follows therefore that a complimentary or completely different mechanism may underlie the high strengths in these alloys systems. Considering the remarkable consistence between the fingerprints for planar slip and the dislocation configuration in the basal orientation of the Mg-Gd alloy, we surmise that the high CRSS in the alloy is directly related to the SRO domains revealed by the x-ray/HR-HAADF-STEM measurements in section 3.1. SRO is known to cause significant strengthening because the leading dislocations experiences the high-energy barrier associated with the creation of the APB. The energy of the anti-phase boundary (APBE) represents the resistance that must be overcome for slip to occur. It is well established that this energy and by extension, the CRSS associated with this mechanism is significantly higher than that associated with solution strengthening [31-35, 52].

Conversely, the analyses in section 3.3 clearly demonstrates that there is remarkable similarity in the stress-strain response/defect structures in the alloy and the pure Mg sample oriented for pyramidal slip. Our results show that $\langle c + a \rangle$ dislocation segments lie predominantly on pyramidal planes, not just in the RE-based alloy as previously reported for macroscopic tests [12], but also in pure Mg. Moreover, our observation is in very good agreement with *in-situ* TEM observations made by Liu and co-workers [47]; they also observed abundant $\langle c + a \rangle$ activity and glide in the pure Mg single crystal they tested. Besides, it is noteworthy that strain hardening is equally high in both systems. We expect that it would be lower in the alloy if the addition of RE elements indeed inhibits the inimical pyramidal II-to-basal transition that is said to underlie the high strain hardening and poor ductility observed in pure Mg [54]. Another important observation is the heterogeneity of pyramidal slip in both pure Mg and Mg-Gd alloy. No evidence of planar slip can be found in the 2B-BF STEM micrographs in Figure 4 (c&d). From a phenomenological point of view, we can imagine that slip will be non-planar in this

orientation because the arrangement of the atoms in the pyramidal planes should preclude the occurrence of planar slip. As illustrated in Figure 9, the SRO will be unaffected by a glide along the pyramidal slip direction, a_1. Furthermore, the length of the $\langle c + a \rangle$ Burgers vector will remain unchanged unlike the case for glide along the basal planes, where the length of the $\langle a \rangle$ burgers vector is effectively doubled to ensure a net zero change in order. We reckon that the non-planarity of slip in this orientation also partly accounts for the comparatively low increase (1.1-fold) in the CRSS for pyramidal slip in the alloy, i.e., relative to the fivefold- and eightfold-increase in basal and twinning CRSS, respectively. Besides, as shown in Figure 10, two- to three-fold increases in the CRSS for pyramidal slip have been reported for Mg-Zn [55] and Mg-Al [45] alloys. We will highlight the implications of these observations on the ductility of the alloy shortly.

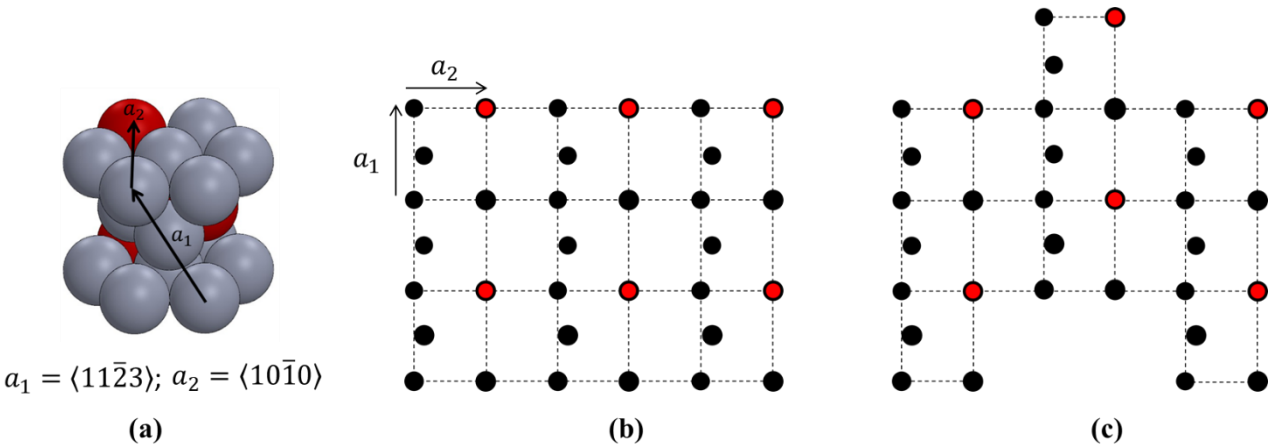

Figure 9 (a) HCP 3D structure with one $\langle 11\bar{2}3 \rangle$ *and* $\langle 10\bar{1}0 \rangle$ *direction highlighted. Schematic of the atomic arrangement in the pyramidal planes (b) before (c) after shear.*

The defect structures in the twinning orientation of the pure Mg sample and the alloy are also very similar, the main difference being the LAGB within the twinned region of the alloy. More importantly, we note that there is no evidence of planar slip in both systems in this orientation, see the 2B-BF STEM micrographs in Figure 7. Notwithstanding, an eightfold increase of the twinning CRSS, and a concomitant delay in twinning that can also be ascribed to the presence of SRO, was observed. Different authors [52, 56, 57] have analysed the structures produced by twins in materials with ordered phases and concluded that ordering significantly reduces the tendency for twinning since it requires the destruction of the order. They argue that the long distance atomic shuffling required to achieve the mirror symmetry between the parent lattice and the twin makes twinning unfavourable in these materials. A number of experimental work on deformation twinning in ordered materials with $D0_{19}$ structure [56, 58, 59], which is precisely comparable to the arrangement of the RE clusters in Mg [25, 38], also support the view that ordering makes it more difficult for twinning to occur. In light of these

reports and the observations made in this work, we conclude that the high twinning CRSS is a consequence of the Gd-rich SRO clusters in the alloy. As previously discussed in section 3.4, non-RE based Mg alloys, e.g. Mg-Al [45], which do not exhibit SRO show significantly smaller increase in twinning CRSS upon alloying.

4.2 Influence of the SRO clusters on ductility

The pyramidal/basal slip (P/B) and twin growth/basal slip (T/B) CRSS ratios for the material systems tested in this work are presented in Figure 10(a) and (b), respectively. The plot also contains the CRSS ratios reported for other Mg systems tested with the microcompression method. We note that there is good agreement between the CRSS ratios for pure Mg in this work and those reported by Li and co-workers [55]. More importantly, our results show that the P/B CRSS ratio of Mg decreased dramatically, by fourfold, upon alloying with 0.75 at.% Gd. Similar drastic decrease in P/B CRSS ratio has also been reported for a micro-compressed Mg-1.13 at.% Y alloy [8]. In contrast, the P/B CRSS ratios are significantly higher in the non-RE based systems, i.e. for the Mg-4 at.% Al, Mg-9 at.% Al and Mg-2 at.% Zn, referenced in Figure 10. Apparently, the fivefold SRO-meditated increase in the CRSS for basal slip in the alloy, along with the more moderate (1.1-fold) increase in pyramidal CRSS, underlies the dramatic decrease in the P/B CRSS ratio and ultimately, the increased $\langle c + a \rangle$ activity observed in deformed Mg-RE polycrystals. It is widely accepted that an increase in the CRSS for basal slip significantly reduces the P/B CRSS ratio, which is prohibitively high in pure Mg and classical Mg alloys [8, 10, 12, 45, 55]. A high P/B CRSS ratio leads to poor ductility in polycrystals since it effectively impedes the activation of the $\langle c + a \rangle$ slip systems, which are essential to satisfy the condition prescribed by von Mises for homogeneous deformation and hence high ductility [13].

On the flip side, it is generally accepted that short range ordering typically leads to a loss in ductility because of its tendency to restrict cross-slip and promote slip planarity [52, 60]. Our results does however indicate that SRO can actually lead to improvement in ductility under the condition described in the preceding paragraph. We thus assert that the influence of the SRO-mediated decrease in the P/B CRSS ratio and the concomitant increase in $\langle c + a \rangle$ activity far outweighs the negative effects of planar slip.

Figure 10(b) also shows that the T/B CRSS ratio of the Mg-Gd alloy is slightly higher than those of pure Mg and the non-RE based Mg alloys except Mg-9 at.% Al. We do not expect this to lead to a decrease in ductility in Mg-Gd since the expected increase in $\langle c + a \rangle$ activity more than likely compensates for the reduced tendency for twinning.

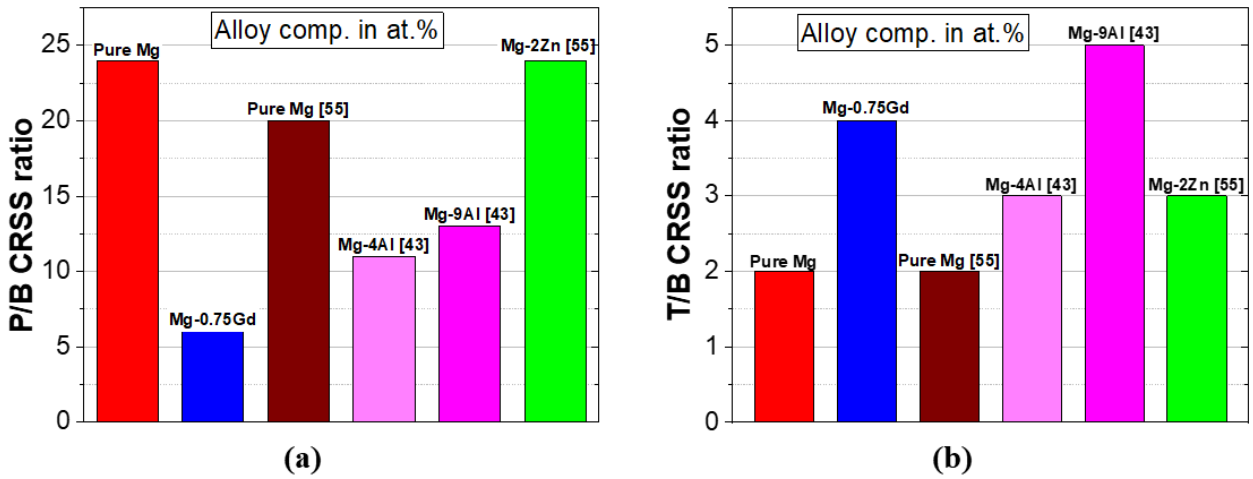

Figure 10: (a) pyramidal-/basal-slip (P/B)– (b) twin growth/basal slip (T/B)– CRSS ratios for material systems tested in this work and those reported for other Mg systems tested with the microcompression method. All compositions are in at.%.

5 Summary

Different mechanistic models have been proposed to rationalize the high room temperature strengths and ductility of low concentration Mg-RE based alloys but these are still open to debate because of gaps between the prediction of these models and experimental results. Moreover, because many of these models rely on experiments carried out in polycrystals, it is difficult to unambiguously decouple the influences of the various microstructural components therein. We circumvented this by compressing single crystal micropillars made in similar orientations in a homogenized Mg-0.75 at.% Gd alloy and in pure Mg. We then carefully analysed the dislocation and twinning structures in cross-sections excised from the deformed pillars. Our investigations show that the deformation mechanisms in both material systems are essentially the same except in the basal orientations, where slip was found to be planar in the alloy but wavy in pure Mg. We show that the planar slip is a consequence of the interactions between dislocations and SRO clusters that exist in the Mg-Gd alloy. 2D X-ray diffraction and HR-HAADF-STEM measurements clearly confirmed the presence of the SRO clusters. Our results also reveal an approximately fivefold fold increase in the basal CRSS of the alloy along with a fourfold decrease of its P/B CRSS ratio, i.e. in comparison with that of pure Mg. Furthermore, we report an eightfold increase in the CRSS for twinning in the alloy. We demonstrate that the Gd-rich SRO clusters in the alloy mediate these changes. We argue that these SRO mediated changes will lead to increased strength and $\langle c + a \rangle$ activity, and ultimately improvements in ductility, in homogenised polycrystalline Mg-Gd alloys.

We note that there is sufficient evidence in literature that the ductility of polycrystals also depends on other factors, such as grain size and texture [6]. Therefore, we imagine that other mechanisms may

additionally contribute to the improvements in the ductility observed in the polycrystalline Mg-RE based alloys. However, our results show that alloying which promotes atomic scale short range ordering, such as seen in Mg-RE based alloys, does significantly enhance strength and ductility.

Acknowledgements:

Access to the Thermofischer-FEI Spectra 300 electron microscope at the user facility in Ernst Ruska-Centre (Forschungszentrum Jülich GmbH, Germany) was granted under the project [ER-C D-074].

Mr. George Diyoke of Institute of Materials Mechanics, Helmholtz Zentrum Hereon, 21502 Geesthacht, Germany, is appreciated for the 3D drawings used in the work.

References

[1] P.G. Partridge, The crystallography and deformation modes of hexagonal close-packed metals, Metallurgical Reviews 12(1) (1967) 169-194.
[2] A. Akhtar, E. Teghtsoonian, Solid solution strengthening of magnesium single crystals—I alloying behaviour in basal slip, Acta Metallurgica 17(11) (1969) 1339-1349.
[3] K.E. Prasad, K. Rajesh, U. Ramamurty, Micropillar and macropillar compression responses of magnesium single crystals oriented for single slip or extension twinning, Acta Materialia 65 (2014) 316-325.
[4] E. Lilleodden, Microcompression study of Mg (0001) single crystal, Scripta Materialia 62(8) (2010) 532-535.
[5] V. Herrera-Solaz, P. Hidalgo-Manrique, M.T. Pérez-Prado, D. Letzig, J. Llorca, J. Segurado, Effect of rare earth additions on the critical resolved shear stresses of magnesium alloys, Materials Letters 128 (2014) 199-203.
[6] K.K. Alaneme, E.A. Okotete, Enhancing plastic deformability of Mg and its alloys—A review of traditional and nascent developments, Journal of Magnesium and Alloys 5(4) (2017) 460-475.
[7] S. Sandlöbes, S. Zaefferer, I. Schestakow, S. Yi, R. Gonzalez-Martinez, On the role of non-basal deformation mechanisms for the ductility of Mg and Mg–Y alloys, Acta Materialia 59(2) (2011) 429-439.
[8] J. Wu, S. Si, K. Takagi, T. Li, Y. Mine, K. Takashima, Y.L. Chiu, Study of basal < a > and pyramidal < c + a > slips in Mg-Y alloys using micro-pillar compression, Philosophical Magazine 100(11) (2020) 1454-1475.
[9] D. Buey, L.G. Hector, M. Ghazisaeidi, Core structure and solute strengthening of second-order pyramidal 〈c+a〉 dislocations in Mg-Y alloys, Acta Materialia 147 (2018) 1-9.
[10] A. Tehranchi, B. Yin, W.A. Curtin, Solute strengthening of basal slip in Mg alloys, Acta Materialia 151 (2018) 56-66.
[11] L. Tang, W. Liu, Z. Ding, D. Zhang, Y. Zhao, E.J. Lavernia, Y. Zhu, Alloying Mg with Gd and Y: Increasing both plasticity and strength, Computational Materials Science 115 (2016) 85-91.
[12] Z. Wu, R. Ahmad, B. Yin, S. Sandlöbes, W.A. Curtin, Mechanistic origin and prediction of enhanced ductility in magnesium alloys, Science 359(6374) (2018) 447-452.
[13] P.M. Anderson, J.P. Hirth, J. Lothe, Theory of dislocations, Cambridge University Press2017.
[14] S. Sandlöbes, M. Friák, S. Zaefferer, A. Dick, S. Yi, D. Letzig, Z. Pei, L.F. Zhu, J. Neugebauer, D. Raabe, The relation between ductility and stacking fault energies in Mg and Mg–Y alloys, Acta Materialia 60(6) (2012) 3011-3021.
[15] S.R. Agnew, L. Capolungo, C.A. Calhoun, Connections between the basal I1 “growth” fault and 〈c+a〉 dislocations, Acta Materialia 82 (2015) 255-265.
[16] M.H. Yoo, S.R. Agnew, J.R. Morris, K.M. Ho, Non-basal slip systems in HCP metals and alloys: source mechanisms, Materials Science and Engineering: A 319-321 (2001) 87-92.
[17] R. Ahmad, B. Yin, Z. Wu, W.A. Curtin, Designing high ductility in magnesium alloys, Acta Materialia 172 (2019) 161-184.
[18] L. Jiang, J.J. Jonas, R. Mishra, Effect of dynamic strain aging on the appearance of the rare earth texture component in magnesium alloys, Materials Science and Engineering: A 528(21) (2011) 6596-6605.
[19] D. Guan, X. Liu, J. Gao, L. Ma, B.P. Wynne, W.M. Rainforth, Exploring the mechanism of “Rare Earth” texture evolution in a lean Mg–Zn–Ca alloy, Scientific Reports 9(1) (2019) 7152.
[20] N. Stanford, I. Sabirov, G. Sha, A. La Fontaine, S.P. Ringer, M.R. Barnett, Effect of Al and Gd Solutes on the Strain Rate Sensitivity of Magnesium Alloys, Metallurgical and Materials Transactions A 41(3) (2010) 734-743.

[21] T. Wang, J.J. Jonas, H. Qin, S. Yue, Effect of dynamic strain aging on the deformation and twinning behavior of a Mg–2Zn–2Nd alloy, Materials Science and Engineering: A 645 (2015) 126-135.
[22] S. Miura, S. Imagawa, T. Toyoda, K. Ohkubo, T. Mohri, Effect of Rare-Earth Elements Y and Dy on the Deformation Behavior of Mg Alloy Single Crystals, MATERIALS TRANSACTIONS 49(5) (2008) 952-956.
[23] L. Gao, R.S. Chen, E.H. Han, Effects of rare-earth elements Gd and Y on the solid solution strengthening of Mg alloys, Journal of Alloys and Compounds 481(1-2) (2009) 379-384.
[24] A. Kula, K. Noble, R.K. Mishra, M. Niewczas, Plasticity of Mg–Gd alloys between 4 K and 298 K, Philosophical Magazine 96(2) (2016) 134-165.
[25] J.F. Nie, N.C. Wilson, Y.M. Zhu, Z. Xu, Solute clusters and GP zones in binary Mg–RE alloys, Acta Materialia 106 (2016) 260-271.
[26] A.R. Natarajan, A. Van der Ven, A unified description of ordering in HCP Mg-RE alloys, Acta Materialia 124 (2017) 620-632.
[27] M. Nishijima, K. Hiraga, M. Yamasaki, Y. Kawamura, Characterization of β′ Phase Precipitates in an Mg-5 at%Gd Alloy Aged in a Peak Hardness Condition, Studied by High-Angle Annular Detector Dark-Field Scanning Transmission Electron Microscopy, MATERIALS TRANSACTIONS 47(8) (2006) 2109-2112.
[28] J.P. Hadorn, T.T. Sasaki, T. Nakata, T. Ohkubo, S. Kamado, K. Hono, Solute clustering and grain boundary segregation in extruded dilute Mg–Gd alloys, Scripta Materialia 93 (2014) 28-31.
[29] J.-F. Nie, Precipitation and Hardening in Magnesium Alloys, Metallurgical and Materials Transactions A 43(11) (2012) 3891-3939.
[30] M. Bugnet, A. Kula, M. Niewczas, G.A. Botton, Segregation and clustering of solutes at grain boundaries in Mg–rare earth solid solutions, Acta Materialia 79 (2014) 66-73.
[31] Z. Lei, X. Liu, Y. Wu, H. Wang, S. Jiang, S. Wang, X. Hui, Y. Wu, B. Gault, P. Kontis, D. Raabe, L. Gu, Q. Zhang, H. Chen, H. Wang, J. Liu, K. An, Q. Zeng, T.-G. Nieh, Z. Lu, Enhanced strength and ductility in a high-entropy alloy via ordered oxygen complexes, Nature 563(7732) (2018) 546-550.
[32] S. Zhao, R. Zhang, Y. Chong, X. Li, A. Abu-Odeh, E. Rothchild, D.C. Chrzan, M. Asta, J.W. Morris, A.M. Minor, Defect reconfiguration in a Ti–Al alloy via electroplasticity, Nature Materials 20(4) (2021) 468-472.
[33] V. Gerold, H.P. Karnthaler, On the origin of planar slip in f.c.c. alloys, Acta Metallurgica 37(8) (1989) 2177-2183.
[34] H. Ovri, E.T. Lilleodden, New insights into plastic instability in precipitation strengthened Al–Li alloys, Acta Materialia 89 (2015) 88-97.
[35] J.C. Fisher, On the strength of solid solution alloys, Acta Metallurgica 2(1) (1954) 9-10.
[36] D. Kupka, N. Huber, E.T. Lilleodden, A combined experimental-numerical approach for elasto-plastic fracture of individual grain boundaries, Journal of the Mechanics and Physics of Solids 64 (2014) 455-467.
[37] J. Šmilauerová, P. Harcuba, J. Stráský, J. Stráská, M. Janeček, J. Pospíšil, R. Kužel, T. Brunátová, V. Holý, J. Ilavský, Ordered array of ω particles in β-Ti matrix studied by small-angle X-ray scattering, Acta Materialia 81 (2014) 71-82.
[38] M. Nishijima, K. Hiraga, Structural Changes of Precipitates in an Mg-5 at%Gd Alloy Studied by Transmission Electron Microscopy, MATERIALS TRANSACTIONS 48(1) (2007) 10-15.
[39] R. Lin, R. Zhang, C. Wang, X.-Q. Yang, H.L. Xin, TEMImageNet training library and AtomSegNet deep-learning models for high-precision atom segmentation, localization, denoising, and deblurring of atomic-resolution images, Scientific Reports 11(1) (2021) 5386.
[40] K. Lejaeghere, V. Van Speybroeck, G. Van Oost, S. Cottenier, Error Estimates for Solid-State Density-Functional Theory Predictions: An Overview by Means of the Ground-State Elemental Crystals, Critical Reviews in Solid State and Materials Sciences 39(1) (2014) 1-24.

[41] E.W. Kelley, W.F. Hosford, The Deformation Characteristics of Textured Magnesium, Transactions of the metallurgical society of AIME, 1968, pp. 654-660.
[42] Y. Liu, N. Li, M. Arul Kumar, S. Pathak, J. Wang, R.J. McCabe, N.A. Mara, C.N. Tomé, Experimentally quantifying critical stresses associated with basal slip and twinning in magnesium using micropillars, Acta Materialia 135 (2017) 411-421.
[43] J.Y. Wang, N. Li, R. Alizadeh, M.A. Monclús, Y.W. Cui, J.M. Molina-Aldareguía, J. Llorca, Effect of solute content and temperature on the deformation mechanisms and critical resolved shear stress in Mg-Al and Mg-Zn alloys, Acta Materialia 170 (2019) 155-165.
[44] J.W. Edington, Interpretation of Transmission Electron Micrographs, in: J.W. Edington (Ed.), Interpretation of Transmission Electron Micrographs, Macmillan Education UK, London, 1975, pp. 22-23.
[45] J. Wang, J.M. Molina-Aldareguía, J. Llorca, Effect of Al content on the critical resolved shear stress for twin nucleation and growth in Mg alloys, Acta Materialia 188 (2020) 215-227.
[46] S. Ando, M. Tsushida, H. Kitahara, Deformation Behavior of Magnesium Single Crystal in c-Axis Compression and a-Axis Tension, Materials Science Forum 654-656 (2010) 699-702.
[47] B.-Y. Liu, F. Liu, N. Yang, X.-B. Zhai, L. Zhang, Y. Yang, B. Li, J. Li, E. Ma, J.-F. Nie, Z.-W. Shan, Large plasticity in magnesium mediated by pyramidal dislocations, Science 365(6448) (2019) 73-75.
[48] F. Wang, S.R. Agnew, Dislocation transmutation by tension twinning in magnesium alloy AZ31, International Journal of Plasticity 81 (2016) 63-86.
[49] M. Legros, Y. Minonishi, D. Caillard, An in-situ transmission electron microscopy study of pyramidal slip in Ti3Al: II. Fine structure of dislocations and dislocation loops, Philosophical Magazine A 76(5) (1997) 1013-1032.
[50] H. Su, X. Zhou, M. Zhang, S. Zheng, H. Ye, Z. Yang, Atomic-resolution studies on reactions of slip dislocations with {$10\bar{1}1$} twin boundaries and local plastic relaxation in a Mg alloy, Acta Materialia 206 (2021).
[51] L. Wang, J. Sabisch, E.T. Lilleodden, Kink formation and concomitant twin nucleation in Mg–Y, Scripta Materialia 111 (2016) 68-71.
[52] N.S. Stoloff, R.G. Davies, The mechanical properties of ordered alloys, Progress in Materials Science 13 (1968) 1-84.
[53] S.R. Agnew, Deformation mechanisms of magnesium alloys, in: C. Bettles, M. Barnett (Eds.), Advances in Wrought Magnesium Alloys, Woodhead Publishing2012, pp. 63-104.
[54] Z. Wu, W.A. Curtin, The origins of high hardening and low ductility in magnesium, Nature 526(7571) (2015) 62-67.
[55] N. Li, C. Wang, M.A. Monclús, L. Yang, J.M. Molina-Aldareguia, Solid solution and precipitation strengthening effects in basal slip, extension twinning and pyramidal slip in Mg-Zn alloys, Acta Materialia 221 (2021) 117374.
[56] M.H. Yoo, C.L. Fu, J.K. Lee, Deformation twinning in metals and ordered intermetallics-Ti and Ti-aluminides, J. Phys. III France 1(6) (1991) 1065-1084.
[57] J.W. Christian, S. Mahajan, Deformation twinning, Progress in Materials Science 39(1) (1995) 1-157.
[58] L. Song, L. Wang, M. Oehring, X. Hu, F. Appel, U. Lorenz, F. Pyczak, T. Zhang, Evidence for deformation twinning of the D019-α2 phase in a high Nb containing TiAl alloy, Intermetallics 109 (2019) 91-96.
[59] N.S. Stoloff, R.G. Davies, The effect of ordering on the plastic deformation of Mg_3Cd, Transactions of American Society for Metals 57 (1964) 247-260.
[60] C.T. Liu, J.O. Stiegler, Ductile Ordered Intermetallic Alloys, Science 226(4675) (1984) 636-642.